

# Quantum Quintom Cosmology

Behzad Tajahmad<sup>a</sup>

<sup>a</sup>*behzadtajahmad@yahoo.com*

---

## Abstract

This work applies the principles of quantum cosmology to examine models incorporating a quintom field. Specifically, three distinct models are analyzed: a simplified toy model, a model featuring an exponential quintom potential, and one where the quintom field is coupled with a negative cosmological constant. For each case, we study the classical trajectories within the configuration space, present solutions to the Wheeler-DeWitt equation in quantum cosmology, and discuss physical interpretations and consequences. A key focus is the behavior of wave packets in the minisuperspace framework. Notably, the correspondence principle (connection between classical and quantum solutions) is also demonstrated.

---

## Contents

<b>1</b>	<b>Introduction</b>	<b>3</b>
<b>2</b>	<b>Classical Quintom Cosmology</b>	<b>6</b>
2.1	Classical equations of motion . . . . .	7
2.2	Classical quintom trajectory for no quintom potential . . . . .	9
2.3	Classical quintom trajectory for interacting exponential scalar field potential and vanishing cosmological constant . . . . .	11
2.4	Classical quintom trajectory for scalar field fluid and negative cosmological constant . . . . .	14
<b>3</b>	<b>Quantum Quintom Cosmology</b>	<b>17</b>
3.1	Wheeler-DeWitt equation and quintom duality . . . . .	17
3.2	Quantum quintom cosmology for no quintom potential . . . . .	18
3.3	Quantum quintom cosmology for interacting exponential potential and vanishing cosmological constant . . . . .	21
3.4	Quantum quintom cosmology for scalar field fluid and negative cosmological constant . . . . .	26
<b>4</b>	<b>Conclusion</b>	<b>30</b>

## 1. Introduction

Current trends in our universe indicate that its expansion is accelerating [1]. We are still in the process of trying to identify a fundamental type of matter that can account for this phenomenon, since any of the forms of matter we are aware of cannot explain it. As a result, the name “dark energy” was given to this form of matter that occupies a dominant portion of the universe’s energy density. The cosmological constant is probably the easiest and most well-known candidate for such a matter, but theoretical physics provides a much wider range of possibilities. Scalar fields with appropriate kinetic and potential energies are one of them.

Dark energy is defined by its negative pressure, which drives the repulsion of matter across the universe and results in its accelerated expansion. Within the framework of general relativity’s standard energy conditions, dark energy must violate the strong energy condition expressed as  $\rho + 3P > 0$  and  $\rho > 0$ . By adopting a barotropic equation of state for the matter in the universe, given as  $P = \omega\rho$  (where  $\omega$  is a constant, and  $P$  and  $\rho$  represent the pressure and density of dark energy, respectively), this implies that  $\omega < -1/3$ . Recent observations demonstrate that dark energy is increasingly inclined toward larger negative values of the barotropic index,  $\omega \leq -1$  while in the past it was greater than  $-1$ . This conclusion remains consistent regardless of whether the assumption of a flat universe [2, 3, 4] is applied or not [5]. Such a scenario implies a violation of the null energy condition [6],  $\rho + P > 0$ , alongside other related energy conditions like the weak energy condition ( $\rho > 0$ ,  $\rho + P > 0$ ) and the dominant energy condition ( $\rho > 0$ ,  $-\rho < P < \rho$ ). Dark energy of this nature has been designated as “phantom” [7, 8, 9]. A phantom can be modeled by a scalar field with negative kinetic energy, often referred to as a “ghost field”. While phantom fields raise theoretical challenges [10], they remain observationally viable candidates for dark energy and justify deeper exploration. Notably, there are phantom field frameworks without pathological behavior in the ultraviolet regime [11]. Phantom models present a unique cosmological phenomenon known as a “big-rip singularity” [7, 8, 9, 12]. Here, energy density and pressure diverge as the scale factor  $a(t)$  grows unbounded within a finite time. This contrasts with an ordinary big crunch singularity, where energy density and pressure become infinite as the scale factor approaches zero. Another intriguing possibility is the “big brake”, characterized by an expansion rate of zero and an acceleration rate plunging to minus infinity [13]. In addition, more exotic types

of singularities might emerge, such as the sudden future singularity [14] and its generalized version [15]—where higher-order derivatives of the scale factor blow up while the scale factor and energy density evolve smoothly—the type III singularity [16], and the type IV singularity [17], both of which also exhibit smooth evolution of the scale factor. Compared to a big rip, these singularities possess less severe characteristics.

Dark energy must evolve to get across  $\omega = -1$ ; this is a great challenge to current cosmology. For positive potential, in the quintessence model,  $\omega$  is always in the range  $-1 \leq \omega \leq 1$ . On the other hand, for the phantom whose kinetic term is the opposite of that of the quintessence, one always has  $\omega \leq -1$ . Neither the quintessence nor the phantom alone can fulfill the transition from  $\omega = -1$ . For k-essence [18], while it is possible to have both  $\omega < -1$  and  $\omega \geq -1$ , it has been indicated in ref. [19] that achieving a transition of  $\omega$  across  $-1$  during the evolution of the universe is highly challenging. To address this, a new dark energy scenario known as quintom was introduced in ref. [20], which combines an ordinary scalar field with a phantom field. This model permits  $\omega$  to cross ‘ $-1$ ’ over time. The quintom model is classified as one of the dynamical dark energy frameworks [21, 22, 23], originally proposed to tackle the issue of accelerated cosmic expansion. However, such models need to be rigorously examined across various stages of the universe’s evolution to determine whether they can form a unified cosmological model. Quintom models, as well as multi-scalar field approaches in general, have been extensively studied in the academic literature—see refs. [24, 25, 26, 27, 28] for further insights.

In these studies, the concept of an evolving universe has traditionally been addressed through classical cosmology, without incorporating the effects of quantum theory on the universe as a whole. The aim of this paper is to bridge that gap by exploring quantum cosmology in the context of a quintom field. This focus stems from the widespread acceptance, supported by both experimental and theoretical evidence, that quantum theory holds universal validity [29]. Consequently, it follows that the universe, in its entirety, should also be described within the framework of quantum theory. If quintom field indeed plays a significant role in cosmic evolution, it becomes essential to examine whether it introduces deviations from the standard approach to quantum cosmology and to analyze any resulting physical implications.

Quantum cosmology fundamentally relies on a theory of quantum gravity [30]. Potential candidates for such a theory include string theory, loop quantum gravity, and quantum geometrodynamics. Like many studies in

quantum cosmology, our current analysis is grounded in the Wheeler-DeWitt equation derived from quantum geometrodynamics. Regardless of the ultimately correct theory of quantum gravity, this approach should provide a sufficiently accurate framework, at least for energy scales below the Planck scale (if not universally (i.e., all scales)). However, as one approaches the Planck scale, alternative models such as loop quantum cosmology [31] might become relevant. Our investigations do not incorporate such modifications and are confined to the current framework, with further elaborations planned for future work.

One key aspect of the Wheeler-DeWitt equation is its local hyperbolic signature [30]. In areas of configuration space close to closed Friedmann cosmologies, the equation exhibits global hyperbolicity, signifying that the kinetic term contains only a single minus sign [32]. This negative contribution to the kinetic term is associated with the scale factor in the Friedmann model, effectively allowing the scale factor to act as a phantom field in a specific sense. The occurrence of an indefinite kinetic term is fundamentally tied to the inherent attractive nature of gravity [33]. Apart from its hyperbolic nature, the defining characteristic of the Wheeler-DeWitt equation is its lack of dependence on an external time parameter [30]. This feature applies, in fact, to any system that exhibits reparametrization invariance at the classical level. Consequently, a coherent approach to quantum cosmology must rely on the intrinsic structure of this equation, steering clear of adopting an intuitive yet incorrect notion of an external Newtonian time. To achieve this, it becomes essential to analyze classical trajectories within a configuration space where the classical time parameter  $t$  has been eliminated. The Wheeler-DeWitt equation's structure plays a crucial role in setting boundary conditions within quantum cosmology. In the hyperbolic case, the equation takes the form of a wave equation, suggesting that boundary conditions should be imposed at constant values of the scale factor. This becomes particularly significant when constructing wave packets that follow classical trajectories in configuration space, resembling standing tube-like structures [34, 35]. Moreover, it is essential for interpreting the pre- and post-big-bang phases in quantum string cosmology [36]. The inclusion of a phantom field alters the structure of the Wheeler-DeWitt equation significantly. When the phantom field dominates alongside the scale factor, the equation takes on an elliptic form. In more general situations, however, the equation transitions to a mixed, or ultrahyperbolic, nature. This structural shift directly impacts the formulation of boundary conditions. A comprehen-

sive analysis of quantum phantom cosmology can be found in ref. [38]. In this paper, we focus on presenting the formal framework for quantum quintom cosmology—incorporating both canonical and phantom fields—along with an exploration of its key physical implications.

The structure of our paper is as follows. Section 2 focuses on the study and resolution of the classical equations of motion for the quintom field in a Friedmann universe. After introducing the necessary equations, we present solutions for the classical trajectories in configuration space across three specific models: a simplified toy model with a vanishing phantom potential; a model incorporating an interacting exponential quintom potential (in multiplicative mode); and a model featuring a cosh-potential (in collective mode) combined with a negative cosmological constant. In Section 3, we extend the discussion to the quantum theory corresponding to these models, following the same sequence. We solve the Wheeler-DeWitt equation exactly for both the toy model and the model with the exponential potential. Notably, we explore wave packet solutions and highlight that quantum effects become significant near the classical big-rip singularity, indicating that such effects manifest prominently on large scales. Since the solutions to the Wheeler-DeWitt equation remain regular in this region, the classical big-rip singularity is effectively eliminated within the quantum framework. Additionally, in realistic scalar field models, the wave function vanishes at the big bang, thereby excluding this singularity in the quantum theory as well. The paper concludes with a summary of our main findings and results.

## 2. Classical Quintom Cosmology

In this section, we first obtain the classical equations and then consider classical quintom trajectories in three models separately:

- No quintom potential (i.e., vanishing quintom potential and vanishing cosmological constant);
- Interacting exponential scalar field potential of quintom and vanishing cosmological constant;
- Scalar field fluid and negative cosmological constant.

The reason for considering classical behavior is that when we acquire quantum solutions in the next section, we have a criterion for taking into account the correspondence principle (leading to classical behavior at  $\hbar \rightarrow 0$ ).

### 2.1. Classical equations of motion

We consider the Friedmann universe characterized by the scale factor  $a(t)$  and two homogeneous scalar fields: a canonical scalar field  $\varphi_1(t)$  and a phantom scalar field  $\varphi_2(t)$ . In this scenario, we assume that both the canonical and phantom fields dominate significantly over any other matter degrees of freedom, leaving them as the primary dynamical components alongside the scale factor. As a result, the configuration space for the system is described by  $\{a, \varphi_1, \varphi_2\}$ . The action governing this setup is expressed as follows:

$$S = \frac{3}{\kappa^2} \int dt N \left( -\frac{a\dot{a}^2}{N^2} + \mathcal{K}a - \frac{\Lambda a^3}{3} \right) + \frac{1}{2} \int dt N a^3 \left( \frac{\dot{\varphi}_1^2 - \dot{\varphi}_2^2}{N^2} - 2V(\varphi_1, \varphi_2) \right), \quad (1)$$

in which the dot denotes a differentiation with respect to time  $t$ . In this context,  $\kappa^2 = 8\pi G$ , where  $G$  represents the gravitational constant, and  $N$  denotes the lapse function. The term  $\mathcal{K} = 0, \pm 1$  corresponds to the curvature index, indicating whether the spatial geometry is flat ( $\mathcal{K} = 0$ ), closed ( $\mathcal{K} = +1$ ), or open ( $\mathcal{K} = -1$ ). The symbol  $\Lambda$  stands for the cosmological constant, while  $V(\varphi_1, \varphi_2)$  refers to the potential associated with the quintom fields. For simplicity, the speed of light has been set to 1.

By assigning  $N = 1$ , the time parameter corresponds to the standard Friedmann cosmic time. Consequently, the action (1) simplifies to:

$$S = \frac{3}{\kappa^2} \int dt \left( -a\dot{a}^2 + \mathcal{K}a - \frac{\Lambda a^3}{3} \right) + \frac{1}{2} \int dt a^3 (\dot{\varphi}_1^2 - \dot{\varphi}_2^2 - 2V(\varphi_1, \varphi_2)). \quad (2)$$

The canonical conjugate momenta corresponding to the scale factor and the scalar fields are given by:

$$\Pi_a = -\frac{6a\dot{a}}{\kappa^2}, \quad \Pi_{\varphi_1} = a^3\dot{\varphi}_1, \quad \Pi_{\varphi_2} = -a^3\dot{\varphi}_2. \quad (3)$$

According to (2), the associated Hamiltonian  $\mathcal{H}$  reads

$$\mathcal{H} = -\frac{\kappa^2}{12a}\Pi_a^2 + \frac{1}{2a^3}\Pi_{\varphi_1}^2 - \frac{1}{2a^3}\Pi_{\varphi_2}^2 + \frac{a^3}{\kappa^2}\Lambda + a^3V - \frac{3a}{\kappa^2}\mathcal{K}. \quad (4)$$

As is customary, the Hamiltonian is set to vanish, meaning  $\mathcal{H} \equiv 0$ . Utilizing (3), one easily finds that this constraint is identical to Friedmann equation:

$$H^2 = \frac{\kappa^2}{3}\rho + \frac{\Lambda}{3} - \frac{\mathcal{K}}{a^2}. \quad (5)$$

where  $H = \dot{a}/a$  represents the Hubble parameter, and  $\rho$  denotes the energy density of the quintom field, which is defined as:

$$\rho \equiv \frac{1}{2}\dot{\varphi}_1^2 - \frac{1}{2}\dot{\varphi}_2^2 + V(\varphi_1, \varphi_2). \quad (6)$$

When  $|\dot{\varphi}_1| > |\dot{\varphi}_2|$ , representing the Canonical scalar Field Dominated (CFD) epoch, the configuration space lacks classically forbidden regions. This is due to the indefiniteness of the total kinetic term. In contrast, if  $|\dot{\varphi}_1| < |\dot{\varphi}_2|$ , which corresponds to the Phantom scalar Field Dominated (PFD) regime, the negative definiteness of the total kinetic term ensures that only a specific region remains classically permitted:

$$V(\varphi_1, \varphi_2) + \frac{\Lambda}{\kappa^2} - \frac{3}{\kappa^2} \frac{\mathcal{K}}{a^2} \geq 0. \quad (7)$$

The ordinary and phantom scalar fields obey the Klein-Gordon equations, which are obtained by varying action (2) with respect to  $\varphi_1$  and  $\varphi_2$ , respectively:

$$\ddot{\varphi}_1 + 3H\dot{\varphi}_1 + \frac{\partial V}{\partial \varphi_1} = 0, \quad (8)$$

$$\ddot{\varphi}_2 + 3H\dot{\varphi}_2 + \frac{\partial V}{\partial \varphi_2} = 0. \quad (9)$$

Assuming a perfect-fluid energy-momentum tensor, the pressure of the quintom field can be defined as:

$$P \equiv \frac{1}{2}\dot{\varphi}_1^2 - \frac{1}{2}\dot{\varphi}_2^2 - V(\varphi_1, \varphi_2). \quad (10)$$

Now, it may easily be understood that equations (8)-(9) are equivalent to the conservation equation:  $\dot{\rho} + 3H(\rho + P) = 0$ . Note that the conservation equation for cosmological constant  $\Lambda$  is fulfilled through another equation of state which is expressed as:  $P_\Lambda = -\rho_\Lambda = -\Lambda/\kappa^2$ .

By the use of (5), the second-order equation for the scale factor is obtained:

$$\dot{H} + H^2 = -\frac{\kappa^2}{6}(\rho + 3P) + \frac{\Lambda}{3}. \quad (11)$$

By employing (6) and (10) and considering a constant barotropic index  $\omega$ , one can readily derive a relationship connecting the quintom potential to



the quintom scalar field:

$$V(\varphi_1, \varphi_2) = \frac{1 - \omega}{1 + \omega} \left( \frac{1}{2} \dot{\varphi}_1^2 - \frac{1}{2} \dot{\varphi}_2^2 \right), \quad \omega \neq -1. \quad (12)$$

Hence, a similar result is found with the virial theorem, according to which the kinetic energy is proportional to the potential energy of the field.

### *2.2. Classical quintom trajectory for no quintom potential*

In this subsection, we aim to explore a simplified model where the cosmological constant is set to zero ( $\Lambda = 0$ ) and the quintom potential vanishes,  $V(\varphi_1, \varphi_2) = 0$ . The associated equation of state,  $\omega$ , takes a value of 1, corresponding to stiff matter characterized by  $P = \rho$ . This behavior stands in stark contrast to the current state of the universe. However, such an evolutionary scenario might be valid in ekpyrotic or cyclic cosmological models, where this type of matter could dominate during the collapsing phase of the universe’s evolution [39].

For the PFD case, a negative energy density under these assumptions renders the model unsuitable for representing dark energy, which is conventionally associated with a positive energy density. Despite violating all known energy conditions, the model intriguingly exhibits certain phantom-like features and benefits from being mathematically straightforward. On the other hand, for the CFD case, while the energy density is positive and aligns with expectations for dark energy, the pressure remains problematic—it should be negative for dark energy but fails to meet this criterion, making this case similarly flawed. Consequently, this model serves merely as a theoretical exercise or “toy model” to examine underlying features. Notably, as we will show, this toy model demonstrates characteristics reminiscent of a “big rip” scenario in configuration space, making it an interesting exploratory framework. We will address more realistic models in subsequent subsections.

In order to acquire classical solutions within the quintom framework, we have to impose  $\mathcal{K} = -1$  in the condition outlined in (7). If  $\mathcal{K}$  is instead set to 0, it becomes evident during calculations that at least one of the scalar fields would emerge as a purely imaginary function. This outcome leads to complications involving a double scalar field problem—phantom or ordinary—rather than a viable quintom model. In this work, we focus exclusively on configurations involving the quintom field.

One of the primary goals of this study is to construct wave packets using the Wheeler-DeWitt equation. For this purpose, it is critical to identify a

classical trajectory within configuration space that eliminates classical time  $t$ . The necessity arises from the absence of such a time parameter in the Wheeler-DeWitt equation.

Owing to the cyclic nature of the variables  $\varphi_1$  and  $\varphi_2$ , the corresponding momentum components  $\Pi_{\varphi_1}$  and  $\Pi_{\varphi_2}$  are conserved quantities. Utilizing equation (3), we reach at:

$$\dot{\varphi}_1^2 = \frac{C_1^2}{a^6}, \quad \dot{\varphi}_2^2 = \frac{C_2^2}{a^6}, \quad (13)$$

where  $C_1$  and  $C_2$  are constants. Consequently, based on equation (5), the following result is obtained:

$$\frac{d\varphi_j}{da} = \pm \frac{|C_j|}{a\sqrt{a^4 + \frac{\kappa^2}{6}(C_1^2 - C_2^2)}}; \quad j = 1, 2, \quad (14)$$

which can be easily integrated to result in

$$\varphi_j = \mp \sqrt{\frac{3}{2}} \frac{|C_j|}{\kappa\sqrt{C_{12}}} \arctan\left(\frac{\sqrt{6a^4 - \kappa^2 C_{12}}}{\kappa\sqrt{C_{12}}}\right), \quad (15)$$

where  $C_{12} = C_1^2 - C_2^2$ , with the assumption that  $|C_1| \neq |C_2|$ . This assumption is straightforward, as it not only prevents the denominator from equating to zero but also ensures that the phantom and canonical scalar fields do not neutralize each other. It is important to note that in the PFD regime (where  $C_{12} < 0$ ) and the CFD regime (where  $C_{12} > 0$ ), after performing a few algebraic manipulations, equation (15) can be respectively simplified to

$$\varphi_j = \pm \sqrt{\frac{3}{2}} \frac{|C_j|}{\kappa\sqrt{|C_{12}|}} \arccos\left(\frac{\kappa\sqrt{|C_{12}|}}{\sqrt{6}a^2}\right), \quad (16)$$

$$\varphi_j = \pm \sqrt{\frac{3}{2}} \frac{|C_j|}{\kappa\sqrt{C_{12}}} \operatorname{arcsinh}\left(\frac{\kappa\sqrt{C_{12}}}{\sqrt{6}a^2}\right). \quad (17)$$

The classical trajectory (eq. 16) has a minimum scale factor value given by  $a_{\min} = \sqrt[4]{\kappa^2|C_{12}|/6}$  and extends to infinite scale factor values at finite scalar field values,  $\varphi_j = \pm \sqrt{\frac{3}{2}} \frac{|C_j|}{\kappa\sqrt{|C_{12}|}} \frac{\pi}{2}$ . As such, it exhibits behaviors resembling a big rip solution. However, it is important to highlight that the scale factor diverges to infinity only as time approaches  $\pm\infty$ . Additionally, the density,  $\rho$ ,

scales proportionally to  $a^{-6}$ , which corresponds to a stiff-fluid density scaling. While this toy model does not fully capture a conventional big rip scenario, it does share some notable characteristics of such behavior in configuration space, making it an intriguing subject of study.

Solution (17) does not contain any turning point; it just demonstrates two branches for which  $a \rightarrow 0$  if  $\varphi_j \rightarrow 0$ , and  $a \rightarrow 0$  if  $\varphi_j \rightarrow \pm\infty$ . The qualitative behaviors of these solutions, eqs. (16)-(17), are illustrated in Figure 1.

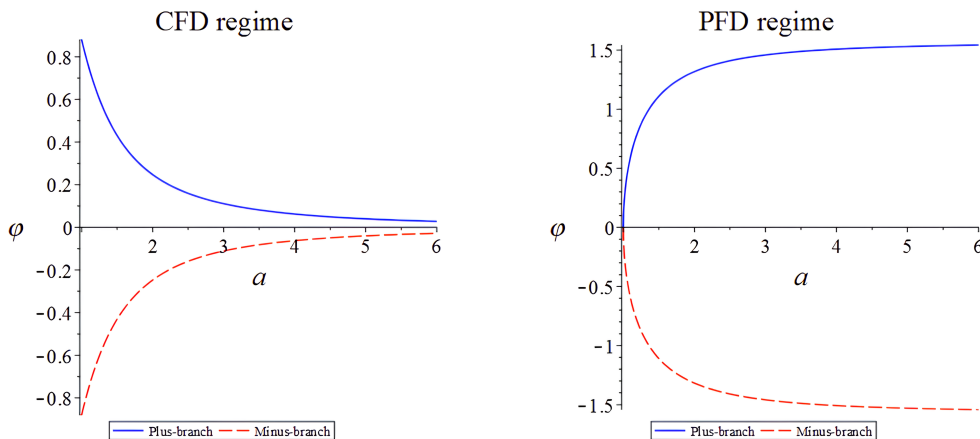


Figure 1: This figure demonstrates the qualitative behaviors of the solutions of PFD regime, (16), CFD regime, (17). In plotting, we have set  $\kappa = \sqrt{6}$ ,  $C_j = 2$ , and  $C_{12} = 1$ .

### 2.3. Classical quintom trajectory for interacting exponential scalar field potential and vanishing cosmological constant

The selection of potential plays a pivotal role in our discussion. Hence, we set it as established in [44]:

$$V(\varphi_1, \varphi_2) = V_0 e^{-\kappa(\lambda_1\varphi_1 + \lambda_2\varphi_2)}, \quad (18)$$

where  $V_0$ ,  $\lambda_1$ , and  $\lambda_2$  represent positive constants. This type of potential has been thoroughly investigated in numerous assisted inflation studies; see, for instance, refs. [40, 41, 42, 43]. As demonstrated in [44], the model under consideration serves as a counterexample to the typical behavior of quintom models with exponential potentials, as it permits the existence

of either tracking attractors (with  $\omega = 0$ ) or phantom attractors (where  $\omega < -1$ ). Exponential potentials commonly arise in frameworks such as Kaluza-Klein theory, supergravity, superstring theory, and higher-order gravity.

In this subsection, we focus on a flat universe where  $\mathcal{K} = 0$ . Based on equation (7), the quintom model does not possess a classically forbidden region. By transforming the classical equations of motion, (8)-(9) and (11), into a dynamical system constrained by the Friedmann equation (5), it becomes evident that this system admits an attractor solution. This solution follows straightforward trajectories in configuration space, as outlined in [44]:

$$\varphi_1(\alpha) = \frac{\lambda_1}{\kappa}\alpha, \quad \varphi_2(\alpha) = -\frac{\lambda_2}{\kappa}\alpha, \quad (19)$$

where  $\alpha \equiv \ln(a)$ . The condition for the existence of this attractor point is given by  $\lambda_1^2 - \lambda_2^2 < 1$ . Additionally, the point is stable if  $\lambda_1 < \sqrt{(1 + \lambda_2^2)/2}$ ; otherwise, it becomes unstable. While the exact solutions were not explicitly derived in ref. [44], they can be straightforwardly determined as follows:

$$\varphi_1 = \frac{2\lambda_1}{(\lambda_1^2 - \lambda_2^2)\kappa} \ln \left[ 1 + \frac{(\lambda_1^2 - \lambda_2^2)H_0}{2}(t - t_0) \right], \quad (20)$$

$$\varphi_2 = \frac{-2\lambda_2}{(\lambda_1^2 - \lambda_2^2)\kappa} \ln \left[ 1 + \frac{(\lambda_1^2 - \lambda_2^2)H_0}{2}(t - t_0) \right], \quad (21)$$

$$\frac{a}{a_0} = \left[ 1 + \frac{(\lambda_1^2 - \lambda_2^2)H_0}{2}(t - t_0) \right]^{\frac{2}{\lambda_1^2 - \lambda_2^2}}, \quad (22)$$

where  $H_0$ ,  $a_0$ , and  $t_0$  are constants. Utilizing (5) and (6) and expressing (5) in the form<sup>1</sup>

$$E_{\text{kin},\varphi_1} - E_{\text{kin},\varphi_2} + E_{\text{pot.}} = 1,$$

the components of kinetic energy and the resulting effective kinetic energy corresponding to the attractor solution mentioned above are respectively

---

<sup>1</sup>Nowhere in this paper does the comma index refer to differentiation, but merely to dependence.

given by:

$$E_{\text{kin.},\varphi_j} = \frac{\kappa^2}{6} \left( \frac{d\varphi_j}{d\alpha} \right)^2 = \frac{\lambda_j^2}{6}; \quad j = 1, 2,$$

$$E_{\text{kin.},\text{eff.}} \equiv E_{\text{kin.},\varphi_1} - E_{\text{kin.},\varphi_2} = \frac{\lambda_1^2 - \lambda_2^2}{6}.$$

As a result, they remain constant, which in turn means the potential energy of the quintom field is also unchanging:

$$E_{\text{pot.}} = \frac{\kappa^2 V}{3H^2} = 1 - \frac{\lambda_1^2 - \lambda_2^2}{6}$$

It is useful to define the following sub-potentials:

$$E_{\text{pot.},1} \equiv \frac{1}{2} - \frac{\lambda_1^2}{6}, \quad E_{\text{pot.},2} \equiv \frac{1}{2} + \frac{\lambda_2^2}{6}, \quad (23)$$

$$\implies E_{\text{pot.},\text{eff.}} = E_{\text{pot.},1} + E_{\text{pot.},2} \quad (24)$$

The equation of state parameter of the quintom field would be:

$$\omega = -1 + \frac{1}{3} (\lambda_1^2 - \lambda_2^2). \quad (25)$$

Therefore, for  $\lambda_2 > \lambda_1$ , the quintom field corresponds to a PFD regime, where  $\omega < -1$ . In contrast, when  $\lambda_2 < \lambda_1$  (the CFD regime), the scalar field behaves such that  $\omega > -1$ .

The energy density of quintom field scales as

$$\rho = \rho_0 \left( \frac{a}{a_0} \right)^{\lambda_2^2 - \lambda_1^2},$$

where  $\rho_0$  is constant. Thus, this leads to a big-rip singularity for  $\lambda_2 > \lambda_1$  (PFD case) because in the limit  $t \rightarrow t_1 \equiv t_0 - 2/[(\lambda_1^2 - \lambda_2^2)H_0]$  both the energy density and the scale factor diverge. On the other hand, as  $t \rightarrow \infty$ , both the scale factor and energy density approach zero. This behavior contrasts with the CFD case ( $\lambda_2 < \lambda_1$ ); In the limit  $t \rightarrow t_1$ , the scale factor collapses to zero while the energy density diverges, yielding a big bang. However, for  $t \rightarrow \infty$ , both the scale factor and energy density again diminish to zero.

2.4. *Classical quintom trajectory for scalar field fluid and negative cosmological constant*

In cosmological models featuring a negative cosmological constant, it is possible to derive a straightforward set of classical solutions. Unlike a positive cosmological constant, which induces cosmological repulsion, a negative cosmological constant acts as a source of attraction. This attractive nature can counteract the effects of dark energy with negative pressure, such as that arising from cosmic strings or domain walls. Consequently, models incorporating a negative cosmological constant and specific fluid components can evolve symmetrically between two singularities, with an extremum occurring in between. As will be indicated later, it is even possible for the evolution to occur between two big rips within a finite cosmic time frame.

In this subsection, we consider a flat universe (denoted by  $\mathcal{K} = 0$ ), a negative cosmological constant ( $\Lambda < 0$ ), and a fluid characterized by the barotropic equation of state  $P = \omega\rho$ . By applying the energy conservation equation under these conditions, we arrive at:

$$\rho = C_3 a^{-3(1+\omega)}, \quad (26)$$

where  $C_3$  is constant. By the use of this equation, equations (5) and (11) can be readily solved to determine the scale factor:

$$a(t) = \left[ a_1 \sinh \left( \sqrt{\frac{\Lambda}{3}} \beta t \right) \right]^{1/\beta}, \quad (27)$$

where  $a_1 = \sqrt{\kappa^2 C_3 / \Lambda}$  and  $\beta = 3(1 + \omega)/2$  which is equivalent to

$$a(t) = \left[ a_2 \sin \left( \sqrt{\frac{-\Lambda}{3}} |\beta| t \right) \right]^{1/\beta}, \quad (28)$$

in which  $a_2 = \sqrt{\kappa^2 C_3 / (-\Lambda)}$ . It is important to note that both ‘cosh’ and ‘cos’ are also valid solutions for our system. However, ‘sinh’ proves to be a better option compared to ‘cosh’, as ‘sinh’ represents both decelerated and accelerated eras, whereas cosh only captures the accelerating phase. Nonetheless, we continue with (28) due to our focus on a negative cosmological constant. By employing the definition of  $\beta$ , we can rewrite (12) in the following form:

$$V(\varphi_1(t), \varphi_2(t)) = \frac{3 - \beta}{2\beta} (\dot{\varphi}_1^2 - \dot{\varphi}_2^2) \quad (29)$$

which permits us to write (6) down as

$$\rho = \frac{3}{2\beta} (\dot{\varphi}_1^2 - \dot{\varphi}_2^2) = \frac{3}{\kappa^2} H^2 - \frac{\Lambda}{\kappa^2}. \quad (30)$$

Therefore, we get a constraint equation for the evolution of  $\varphi_1$  and  $\varphi_2$ :

$$\dot{\varphi}_1^2 - \dot{\varphi}_2^2 = -\frac{2\beta\Lambda}{3\kappa^2} \csc^2 \left( \sqrt{\frac{-\Lambda}{3}} |\beta|t \right) \quad (31)$$

If both the canonical and phantom fields are real, the equation represents a hyperbola, while if  $\varphi_1$  is real and  $\varphi_2$  is purely imaginary, the equation corresponds to a circle at a fixed cosmic time. To analyze the system, it is essential to establish a relationship between the ordinary and phantom fields for their proper determination. Notably, in most studies (for instance, see refs. [44, 45]),  $\varphi_1$  and  $\varphi_2$  have been obtained proportional to each other. Based on this, we define  $\varphi_1 = A\varphi_2$ , where  $A$  is a constant. It is important to note that  $A \neq 1$ , as this condition prevents the two fields from canceling each other. By adopting these assumptions, we can proceed to calculate the evolution of the scalar fields as follows:

$$\varphi_1(t) = \frac{\pm\sqrt{2}A}{\kappa\sqrt{|\beta|(A^2-1)}} \ln \left| \tan \left( \sqrt{\frac{-\Lambda}{12}} |\beta|t \right) \right|, \quad (32)$$

$$\varphi_2(t) = \frac{\pm\sqrt{2}}{\kappa\sqrt{|\beta|(A^2-1)}} \ln \left| \tan \left( \sqrt{\frac{-\Lambda}{12}} |\beta|t \right) \right|. \quad (33)$$

Obviously, the argument, i.e.,  $\sqrt{-\Lambda/12} |\beta|t$ , must be between 0 and  $\pi$ . It is worth noting that when the argument becomes an integer multiple of  $\pi$ , a singularity arises.

Considering the fact that  $\beta$  can be expressed as  $(\lambda_1^2 - \lambda_2^2)/2$ , it follows that  $\beta > 0$  corresponds to the CFD scenario, while  $\beta < 0$  pertains to the PFD regime. Pursuant to (28), for a positive  $\beta$ —which signifies a negative cosmological constant combined with an  $\omega > -1$  fluid—the universe evolves from a big bang at  $t = 0$ , reaches a maximum expansion characterized by  $a_{\max.} = a_2^{1/\beta}$ , and ultimately concludes with a big crunch at  $t = \pi$ . In contrast, in the PFD regime (negative  $\beta$ ), the universe begins with a big rip at  $t = 0$ , shrinks to a minimum scale factor  $a_{\min.} = a_2^{-1/|\beta|}$ , and expands toward another big rip at  $t = \pi$ . This evolution in the PFD case is symmetric, making it particularly intriguing from a theoretical perspective. Moreover, this

framework may provide valuable insights into the study of the cosmological arrow of time. Interestingly, similar symmetric behavior can also be observed in the configuration space. By eliminating (28) and (32)-(33) from the expressions for the classical time coordinate, the classical evolution trajectories are derived as follows:

$$\varphi_1(a) = \frac{\pm\sqrt{2}A}{\kappa\sqrt{|\beta|(A^2-1)}} \ln\left(\frac{a^\beta}{a_2 + \sqrt{a_2^2 - a^{2\beta}}}\right), \quad (34)$$

$$\varphi_2(a) = \frac{\pm\sqrt{2}}{\kappa\sqrt{|\beta|(A^2-1)}} \ln\left(\frac{a^\beta}{a_2 + \sqrt{a_2^2 - a^{2\beta}}}\right). \quad (35)$$

From these expressions, we observe the existence of two branches. In the PFD case, both branches extend indefinitely, meaning that as  $a \rightarrow \infty$ , we find  $\varphi_{1,2} \rightarrow \pm\infty$ . Each branch reaches a minimum, where  $\varphi_{1,2}(a) = 0$ , occurring at  $a_{\min} = a_2^{-1/|\beta|}$ . On the other hand, in the CFD regime, it is evident that the system features a maximum value at  $a_{\max}$ . The classical trajectories within the configuration space are illustrated in Figure 2.

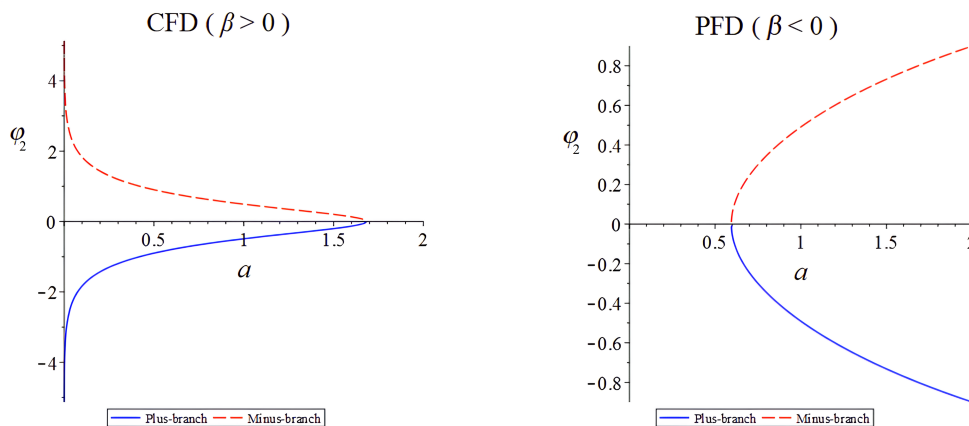


Figure 2: This figure indicates the qualitative behavior of (35) in two regime. In drawing these plots, we have chosen  $\kappa = \sqrt{6}$ ,  $|\beta| = 2$ ,  $A = 2$ , and  $a_2 = \sqrt{8}$ .

Using equations (32)-(33) along with (29), one can straightforwardly reconstruct the form of the quantom potential:

$$V(\varphi_1, \varphi_2) = V_{01} \cosh^2\left(\frac{\varphi_1}{C_{01}}\right) + V_{02} \cosh^2\left(\frac{\varphi_2}{C_{02}}\right), \quad (36)$$



in which

$$C_{01} = \frac{\pm\sqrt{2}A}{\kappa\sqrt{|\beta(A^2 - 1)|}}, \quad C_{02} = \frac{\pm\sqrt{2}}{\kappa\sqrt{|\beta(A^2 - 1)|}}, \quad (37)$$

$$V_{01} = \frac{\beta\Lambda(\beta - 3)}{6}C_{01}^2, \quad V_{02} = -\frac{\beta\Lambda(\beta - 3)}{6}C_{02}^2. \quad (38)$$

Various potential forms have been outlined in refs. [46, 47], according to which this specific type (36) is known as the unified dark matter potential. It is worth noting that in the CFD case, the potential is positive only when  $\beta < 3$  (i.e.,  $\omega < 1$ ).

### 3. Quantum Quintom Cosmology

This section focuses on exploring quantum behavior. For this purpose, the steps and conditions under examination align with those used in classical studies.

#### 3.1. Wheeler-DeWitt equation and quintom duality

As a result of quantizing the Hamiltonian constraint (4), we can obtain the Wheeler-DeWitt equation. Choosing the Laplace-Beltrami factor ordering it turns out to be

$$\left( \frac{\kappa^2 \hbar^2}{12} a \frac{\partial}{\partial a} a \frac{\partial}{\partial a} - \frac{\hbar^2}{2} \frac{\partial^2}{\partial \varphi_1^2} + \frac{\hbar^2}{2} \frac{\partial^2}{\partial \varphi_2^2} + a^6 \left( V(\varphi_1, \varphi_2) + \frac{\Lambda}{\kappa^2} \right) - \frac{3\mathcal{K}a^4}{\kappa^2} \right) \psi(a, \varphi_1, \varphi_2) = 0. \quad (39)$$

Similar to phantom duality which has been defined as [48, 49]

$$a \rightarrow \frac{1}{a}, \quad \varphi \rightarrow -i\bar{\varphi}, \quad (40)$$

where  $i = \sqrt{-1}$ , we may define here quintom duality as follows:

$$a \rightarrow \frac{1}{a}, \quad \varphi_1 \rightarrow -i\bar{\varphi}_1, \quad \varphi_2 \rightarrow -i\bar{\varphi}_2. \quad (41)$$

Under the defined quintom duality, for flat universe,  $\mathcal{K} = 0$ , the Wheeler-DeWitt equation for  $a$ ,  $\varphi_1$ , and  $\varphi_2$ , i.e.,

$$\left( \frac{\kappa^2 \hbar^2}{12} a \frac{\partial}{\partial a} a \frac{\partial}{\partial a} - \frac{\hbar^2}{2} \frac{\partial^2}{\partial \varphi_1^2} + \frac{\hbar^2}{2} \frac{\partial^2}{\partial \varphi_2^2} + a^6 \left( V(\varphi_1, \varphi_2) + \frac{\Lambda}{\kappa^2} \right) \right) \psi(a, \varphi_1, \varphi_2) = 0, \quad (42)$$

transforms into the Wheeler-DeWitt equation for  $\bar{a}$ ,  $\bar{\varphi}_1$ , and  $\bar{\varphi}_2$ , viz.

$$\left( \frac{\kappa^2 \hbar^2}{12} \bar{a} \frac{\partial}{\partial \bar{a}} \bar{a} \frac{\partial}{\partial \bar{a}} + \frac{\hbar^2}{2} \frac{\partial^2}{\partial \bar{\varphi}_1^2} - \frac{\hbar^2}{2} \frac{\partial^2}{\partial \bar{\varphi}_2^2} + \bar{a}^6 \left( V(i\bar{\varphi}_1, i\bar{\varphi}_2) + \frac{\Lambda}{\kappa^2} \right) \right) \psi(\bar{a}, \bar{\varphi}_1, \bar{\varphi}_2) = 0. \quad (43)$$

The transformations for both canonical and phantom fields are thus just a Wick rotation. We will revisit and discuss the results of quintom duality in subsection 3.4.

The natural logarithm of scale factor,  $\alpha = \ln(a)$ , allows eq. (42) to be conveniently rewritten as follows

$$\left( \frac{\kappa^2 \hbar^2}{12} \frac{\partial^2}{\partial \alpha^2} - \frac{\hbar^2}{2} \frac{\partial^2}{\partial \varphi_1^2} + \frac{\hbar^2}{2} \frac{\partial^2}{\partial \varphi_2^2} + e^{6\alpha} \left( V(\varphi_1, \varphi_2) + \frac{\Lambda}{\kappa^2} \right) \right) \Psi(\alpha, \varphi_1, \varphi_2) = 0, \quad (44)$$

We intend to utilize both forms (39) and (44) to work in the next subsections.

### 3.2. Quantum quintom cosmology for no quintom potential

For vanishing cosmological constant and quintom potential and  $\mathcal{K} = -1$ , the Wheeler-DeWitt equation (39) may be obtained by the separation method, viz.

$$\psi_{k_{1,2}}(a, \varphi_1, \varphi_2) = \Upsilon_{k_{1,2}}(a) \phi_{k_1}(\varphi_1) \phi_{k_2}(\varphi_2). \quad (45)$$

We choose

$$\phi_{k_1}(\varphi_1) = e^{-ik_1\varphi_1/\hbar}, \quad \phi_{k_2}(\varphi_2) = e^{-ik_2\varphi_2/\hbar}, \quad (46)$$

because if real exponentials were used, wave functions for  $\varphi_{1,2} \rightarrow \pm\infty$  would exponentially increase, which would not reflect classical behavior. By inserting these selections in (39), one gets the following equation for  $\Upsilon_{k_{1,2}}(a)$ :

$$a^2 \Upsilon_{k_{1,2}}'' + a \Upsilon_{k_{1,2}}' + \frac{1}{\hbar^2} \left( \frac{36}{\kappa^4} a^4 - \frac{6}{\kappa^2} k_3^2 \right) \Upsilon_{k_{1,2}} = 0, \quad (47)$$

where  $k_3^2 = k_2^2 - k_1^2$  and primes denote derivatives with respect to the scale factor  $a$ . For convenience, let us set  $\kappa^2 = 6$ . We begin by examining the PFD case, characterized by  $k_2 > k_1$ , which implies  $k_3 > 0$ . In general, the solutions to the governing equation are given by Bessel functions of the

form  $Z_{k_3/2\hbar}(a^2/2\hbar)$ . However, to ensure the solution reflects the behavior of a classical trajectory, it is necessary to impose a boundary condition such that  $\psi(a, \varphi_1, \varphi_2) \rightarrow 0$  as  $a \rightarrow 0$ . By applying this boundary condition, the path exhibits a minimum in configuration space relative to the scale factor, aligning with classical expectations. To satisfy this condition, we select the Bessel function  $J_{k_3/2\hbar}(a^2/(2\hbar))$ , which corresponds to  $k_3 > 0$ . The connection to the classical solution is achieved via the formal WKB approximation in the limit  $\hbar \rightarrow 0$ . Consequently, it becomes necessary to analyze an asymptotic expansion of  $J$  under the condition that both the argument and the index are large. According to ref. [50], we utilize the following expression:

$$J_\nu(\nu z) = \left( \frac{4\zeta}{1-z^2} \right)^{1/4} \left( \frac{\text{Ai}(\nu^{2/3}\zeta)}{\nu^{1/3}} + \frac{\exp(-\frac{2}{3}\nu\zeta^{3/2})}{1+\nu^{1/6}|\zeta|^{1/4}} \mathcal{O}\left(\frac{1}{\nu^{4/3}}\right) \right), \quad (48)$$

where Ai represents the Airy function, and the specific form of  $\zeta$  depends on whether  $z^2 \geq 1$  or  $z^2 < 1$ . Let us first analyze the case where  $z^2 \geq 1$ . Define  $\nu = k_3/(2\hbar)$  and  $z = a^2/k_3$ . In this scenario (i.e.,  $z^2 \geq 1 \implies a^4/k_3^2 \geq 1$ ), the expression for  $\zeta$  is given by

$$\zeta = - \left( \frac{3}{2} \left( \sqrt{\frac{a^4}{k_3^2} - 1} - \arccos\left(\frac{k_3}{a^2}\right) \right) \right)^{2/3}. \quad (49)$$

Furthermore, it becomes essential to utilize the asymptotic expression for the Airy function, as its argument is also significantly large. Thus we make use [51]:

$$\text{Ai}\left(\left(\frac{k_3}{2\hbar}\right)^{2/3} \zeta\right) \sim \pi^{-1/2} \left(-\left(\frac{k_3}{2\hbar}\right)^{2/3} \zeta\right)^{-1/4} \sin(\theta_{k_3}), \quad (50)$$

in which

$$\theta_{k_3} = -\frac{k_3}{3\hbar}\zeta^{3/2} + \frac{\pi}{4}. \quad (51)$$

Through the principle of constructive interference, the classical trajectory can be recovered. The objective is to identify the point where the phase of the wave function reaches its extremum with respect to  $k$ . The phase is

$$S_{k_{1,2}} \equiv \theta_{k_3} \pm \frac{k_1\varphi_1 + k_2\varphi_2}{\hbar}. \quad (52)$$

The requirements

$$\left. \frac{\partial S_{k_{1,2}}}{\partial k_1} \right|_{k_1=\bar{k}_1} = 0, \quad \left. \frac{\partial S_{k_{1,2}}}{\partial k_2} \right|_{k_2=\bar{k}_2} = 0, \quad (53)$$

yield (16). One may easily identify that  $\bar{k}_3 = \sqrt{|C_{12}|}$ , in which  $\bar{k}_3^2 = \bar{k}_2^2 - \bar{k}_1^2$ , and  $|C_1| = \bar{k}_1$  and  $|C_2| = \bar{k}_2$ . Note that we have set  $\kappa^2 = 6$ .

For the latter one, namely  $z^2 = (a^4/k_3^2) < 1$ , according to the expressions in ref. [51],  $\zeta < 0$  and the corresponding Airy function decays exponentially. This result is not surprising because  $z^2 = (a^4/k_3^2) < 1$  corresponds to the classically forbidden region.

It can be easily indicated that through substitutions  $\Pi_a \rightarrow \partial S_{k_{1,2}}/\partial a$ ,  $\Pi_{\varphi_1} \rightarrow \partial S_{k_{1,2}}/\partial \varphi_1$ , and  $\Pi_{\varphi_2} \rightarrow \partial S_{k_{1,2}}/\partial \varphi_2$ ,  $S_{k_{1,2}}$  is a solution to the Hamilton-Jacobi equation arising from (4).

Now we consider CFD case. Obviously, for this regime, the sign beside  $k_3^2$ -term will change in (47) meaning that we can rewrite it as  $(\pm i k_3)^2$  preserving the structure of (47). Hence, the solutions to  $\Upsilon_{k_{1,2}}(a)$  would be the Bessel functions  $J_{\pm i k_3/(2\hbar)}(a^2/(2\hbar))$ . Both solutions are permissible because no classically forbidden regions exist. Again, the classical trajectory in this case, i.e., (17), like the previous one, is recovered through the principle of constructive interference. As a consequence, one obtains two branches of (17) from two Bessel functions. To suppress interference effects (and thereby avoid nonclassical behavior), it therefore is advisable to select one or the other Bessel function at a large scale factor. Given the hyperbolic nature of (39) in the CFD regime, there is flexibility in imposing boundary conditions at constant scale factors. This choice includes imposing either one wave packet or two wave packets for each scalar field, depending on whether one prefers to demonstrate a single branch or both branches of the classical solution.

For the PFD case, however, the Wheeler-DeWitt equation becomes elliptic. Here, one can only apply boundary conditions such that  $\psi(a, \varphi_1, \varphi_2) \rightarrow 0$  as  $a \rightarrow 0$ , while ensuring that it oscillates at most at other boundaries. This constraint leads to solutions expressed as  $J_{k_3/(2\hbar)}(a^2/(2\hbar))$  or superpositions thereof. To construct a wave packet, one would explicitly consider the following superposition:

$$\psi(a, \varphi_1, \varphi_2) = \int_0^\infty \int_0^\infty dk_1 dk_2 A(k_1) B(k_2) e^{-ik_1 \varphi_1/\hbar} e^{-ik_2 \varphi_2/\hbar} J_{k_3/(2\hbar)}(a^2/(2\hbar)), \quad (54)$$

where  $A(k_1)$  and  $B(k_2)$  are functions of  $k_1$  and  $k_2$  that are sharply localized around specific values  $\bar{k}_1$  and  $\bar{k}_2$ , such as Gaussian profiles. Since the phase of the Bessel function varies slowly with respect to  $k_3$ , it follows that the wave packet would not exhibit significant dispersion near the classical trajectory's minimum—contrasting with the behavior observed in a massive scalar field, as described in ref. [52]. Nevertheless, dispersion phenomena are anticipated for larger scale factors. For a more practical and detailed examination of this scenario, the explicit analysis will be presented in the next subsection.

Drawing an analogy to ordinary quantum mechanics, the solution in the elliptic case can be likened to an initial wave function  $\psi|_{t=0}$ . On the other hand, the hyperbolic case corresponds to the time evolution of the wave function, as equation (39) would feature a distinct set of foliations associated with an intrinsic time defined by  $a$ . This intrinsic time could potentially serve as a physical time, within which other degrees of freedom could evolve dynamically.

### 3.3. Quantum quintom cosmology for interacting exponential potential and vanishing cosmological constant

In subsection 2.3, the quintom model was analyzed for a nonzero interacting exponential potential in a flat universe. Here, we extend the study to its quantum counterpart. To proceed systematically, and without loss of generality, we first assume that the wave function can be expressed as  $\Psi(\alpha, \varphi_1, \varphi_2) = \Psi_1(\alpha, \varphi_1)\Psi_2(\alpha, \varphi_2)$  in equation (44). Under this assumption, the problem reduces to two coupled partial differential equations:

$$\left( \hbar^2 \frac{\partial^2}{\partial \alpha^2} - \hbar^2 \frac{\partial^2}{\partial \varphi_1^2} + e^{6\alpha} V(\varphi_1, \varphi_2) \right) \Psi_1(\alpha, \varphi_1) = 0, \quad (55)$$

$$\left( \hbar^2 \frac{\partial^2}{\partial \alpha^2} + \hbar^2 \frac{\partial^2}{\partial \varphi_2^2} + e^{6\alpha} V(\varphi_1, \varphi_2) \right) \Psi_2(\alpha, \varphi_2) = 0. \quad (56)$$

Since equation (55) primarily addresses the Canonical field and equation (56) emphasizes the Phantom field, we refer to these as the C-part and P-part of the Wheeler-DeWitt equations, respectively. These parts of the Wheeler-DeWitt equation can be effectively solved by implementing transformations to new variables, allowing the effective potential in front of  $\Psi_{1,2}$  in (55) and (56) to be eliminated. This becomes achievable by initially transitioning to

the coordinate sets  $(Q_1, Q_2)$  and  $(Q_3, Q_4)$ , which are defined as follows:

$$\text{For (55)} : \begin{cases} Q_1 \equiv \alpha + \varphi_1 \\ Q_2 \equiv \alpha - \varphi_1 \end{cases} ; \quad (57)$$

$$\text{For (56)} : \begin{cases} Q_3 \equiv \alpha + i\varphi_2 \\ Q_4 \equiv \alpha - i\varphi_2 \end{cases} . \quad (58)$$

These coordinates exhibit a light-cone type structure. It is worth noting that, in this mapping, a degree of freedom is initially added following the transformation. However, due to the relation  $Q_1 + Q_2 = Q_3 + Q_4$ , the system effectively reduces back to three degrees of freedom. Consequently, eqs. (55) and (56) simplify to

$$\begin{aligned} \left( \hbar^2 \frac{\partial^2}{\partial Q_1 \partial Q_2} + F(Q_1, Q_2, Q_3, Q_4) \right) \Psi_1(Q_1, Q_2) &= 0, \\ \left( \hbar^2 \frac{\partial^2}{\partial Q_3 \partial Q_4} + F(Q_1, Q_2, Q_3, Q_4) \right) \Psi_1(Q_3, Q_4) &= 0, \end{aligned}$$

where  $F(Q_1, Q_2, Q_3, Q_4)$  for the potential (18) would be

$$\frac{1}{2} V_0 \exp \left( 3(Q_1 + Q_2) - \sqrt{\frac{3}{2}} [\lambda_1(Q_1 - Q_2) - i\lambda_2(Q_3 - Q_4)] \right)$$

Clearly, we require transformations into new variables that can effectively eliminate  $F$ . These transformations are respectively represented as follows:

$$\begin{cases} u_1(\alpha, \varphi_1, \varphi_2) = 2\sqrt{V_0} \frac{\exp[3\alpha - \sqrt{6}(\lambda_1\varphi_1 + \lambda_2\varphi_2)/2]}{6 - \lambda_1^2} \left( \cosh(X_1) + \frac{\lambda_1}{\sqrt{6}} \sinh(X_1) \right); \\ v_1(\alpha, \varphi_1, \varphi_2) = 2\sqrt{V_0} \frac{\exp[3\alpha - \sqrt{6}(\lambda_1\varphi_1 + \lambda_2\varphi_2)/2]}{6 - \lambda_1^2} \left( \sinh(X_1) + \frac{\lambda_1}{\sqrt{6}} \cosh(X_1) \right); \end{cases} \quad (59)$$

$$\begin{cases} u_2(\alpha, \varphi_1, \varphi_2) = 2\sqrt{V_0} \frac{\exp[3\alpha - \sqrt{6}(\lambda_1\varphi_1 + \lambda_2\varphi_2)/2]}{6 + \lambda_2^2} \left( \cosh(X_2) - i \frac{\lambda_1}{\sqrt{6}} \sinh(X_2) \right); \\ v_2(\alpha, \varphi_1, \varphi_2) = 2\sqrt{V_0} \frac{\exp[3\alpha - \sqrt{6}(\lambda_1\varphi_1 + \lambda_2\varphi_2)/2]}{6 + \lambda_2^2} \left( -i \sinh(X_2) - \frac{\lambda_1}{\sqrt{6}} \cosh(X_2) \right); \end{cases} \quad (60)$$

where

$$X_1 \equiv 3\varphi_1 - \sqrt{\frac{3}{2}} \lambda_1 \alpha, \quad X_2 \equiv i \left( 3\varphi_2 + \sqrt{\frac{3}{2}} \lambda_2 \alpha \right). \quad (61)$$

As a result, the C- and P-parts of the Wheeler-DeWitt equation in these new coordinates turn out to be

$$\hbar^2 \left( \frac{\partial^2 \Psi_1}{\partial u_1^2} - \frac{\partial^2 \Psi_1}{\partial v_1^2} \right) + \Psi_1 = 0; \quad (62)$$

$$\hbar^2 \left( \frac{\partial^2 \Psi_2}{\partial u_2^2} + \frac{\partial^2 \Psi_2}{\partial v_2^2} \right) + \Psi_2 = 0. \quad (63)$$

Utilizing WKB-approximations ansatz,  $\Psi_1 = C_4 \exp(\pm i S_1/\hbar)$  and  $\Psi_2 = C_5 \exp(\pm i S_2/\hbar)$ , we may acquire at lowest order the Hamiltonian-Jacobi equations

$$\left( \frac{\partial S_{01}}{\partial u_1} \right)^2 - \left( \frac{\partial S_{01}}{\partial v_1} \right)^2 = 1, \quad (64)$$

$$\left( \frac{\partial S_{02}}{\partial u_2} \right)^2 + \left( \frac{\partial S_{02}}{\partial v_2} \right)^2 = 1. \quad (65)$$

These equations may be solved through a separation ansatz by

$$S_{01,k_1} = k_1 u_1 - \sqrt{k_1^2 - 1} v_1, \quad S_{02,k_2} = k_2 u_2 - i \sqrt{k_2^2 - 1} v_2. \quad (66)$$

It is also feasible to solve the Hamilton-Jacobi equation by employing actions with differing signs applied to the pairs  $\{u_1, v_1\}$  and  $\{u_2, v_2\}$ . These are obtained from the one chosen above through rotations in the  $(u_1, v_1)$ - and  $(u_2, v_2)$ -planes. In doing so, all solutions may be mapped onto each other for (65) because of the rotational symmetry inherent in this equation. If we set  $\lambda_1 < 6$ , then only two solutions of the C-part may be mapped onto each other.

By the use of the classical actions  $S_{01,k_1}$  and  $S_{02,k_2}$ , the equations of motion take the form:

$$\left. \frac{\partial S_{01,k_1}}{\partial k_1} \right|_{k_1=\bar{k}_1} = C_6, \quad \left. \frac{\partial S_{02,k_2}}{\partial k_2} \right|_{k_2=\bar{k}_2} = C_7.$$

The classical trajectories (19) are recovered through the following special selections, respectively:

$$\bar{k}_1^2 = E_{\text{pot.,1}}^{-1} = \left( \frac{1}{2} - \frac{\lambda_1^2}{6} \right)^{-1}, \quad C_6 = 0;$$

$$\bar{k}_2^2 = E_{\text{pot.,2}}^{-1} = \left( \frac{1}{2} + \frac{\lambda_2^2}{6} \right)^{-1}, \quad C_7 = 0,$$

namely we get

$$\varphi_1(\alpha) = \frac{\lambda_1}{\sqrt{6}}\alpha, \quad \varphi_2(\alpha) = -\frac{\lambda_2}{\sqrt{6}}\alpha. \quad (67)$$

Incorporating this lowest-order ansatz into the Wheeler-DeWitt equations, it can be determined that the equations are already fully satisfied. Consequently, the corresponding exact wave packets for the Wheeler-DeWitt equations are derived as follows:

$$\begin{aligned} \Psi_1(u_1, v_1) = \int dk_1 A(k_1) & \left( C_8 \exp \left[ \frac{i}{\hbar} \left( k_1 u_1 - \sqrt{k_1^2 - 1} v_1 \right) \right] \right. \\ & \left. + C_9 \exp \left[ -\frac{i}{\hbar} \left( k_1 u_1 - \sqrt{k_1^2 - 1} v_1 \right) \right] \right), \end{aligned} \quad (68)$$

$$\begin{aligned} \Psi_2(u_2, v_2) = \int dk_2 B(k_2) & \left( C_{10} \exp \left[ \frac{i}{\hbar} \left( k_2 u_2 - i\sqrt{k_2^2 - 1} v_2 \right) \right] \right. \\ & \left. + C_{11} \exp \left[ -\frac{i}{\hbar} \left( k_2 u_2 - i\sqrt{k_2^2 - 1} v_2 \right) \right] \right), \end{aligned} \quad (69)$$

and the total  $\Psi$  is given by  $\Psi_1\Psi_2$ . Through constructive interference, these equations can be used to recover classical trajectories. We opt for the amplitudes  $A$  and  $B$  Gaussian functions with width  $\sigma$  centered around  $\bar{k}_1$  and  $\bar{k}_2$ , respectively:

$$\begin{aligned} A(k_1) &= \frac{1}{\sqrt[4]{\pi\sigma^2\hbar^2}} \exp \left[ -\frac{(k_1 - \bar{k}_1)^2}{2\sigma^2\hbar^2} \right], \\ B(k_2) &= \frac{1}{\sqrt[4]{\pi\sigma^2\hbar^2}} \exp \left[ -\frac{(k_2 - \bar{k}_2)^2}{2\sigma^2\hbar^2} \right]. \end{aligned}$$

Choosing  $C_8 = C_9$  and  $C_{10} = C_{11}$  for definiteness, we arrive at wave packets of the forms

$$\psi_1(u_1, v_1) \approx C_8 \pi^{1/4} \sqrt{\frac{2\sigma\hbar}{1 - i\sigma^2\hbar S_{01,k_1}^n}} \exp \left[ \frac{iS_{01,k_1}}{\hbar} - \frac{\sigma^2 S_{01,k_1}^2}{2(1 - i\hbar\sigma^2 S_{01,k_1}^n)} \right], \quad (70)$$

$$\psi_2(u_2, v_2) \approx C_{10} \pi^{1/4} \sqrt{\frac{2\sigma\hbar}{1 - i\sigma^2\hbar S_{02,k_2}^n}} \exp \left[ \frac{iS_{02,k_2}}{\hbar} - \frac{\sigma^2 S_{02,k_2}^2}{2(1 - i\hbar\sigma^2 S_{02,k_2}^n)} \right], \quad (71)$$



where the Taylor expansions of  $S_{01,k_1}$  and  $S_{02,k_2}$  have been performed around  $\bar{k}_1$  and  $\bar{k}_2$ , respectively, and for simplicity  $S_{0j,k_j}(\bar{k}_j) \equiv S_{0j,k_j}$  for  $j = 1, 2$ . The math symbols,  $(^i)$ , for  $S_{01,k_1}$  and  $S_{02,k_2}$  denote derivatives with respect to  $k_1$  and  $k_2$ , respectively. It must be mentioned that the terms of the orders  $(k_1 - \bar{k}_1)^3$  and  $(k_2 - \bar{k}_2)^3$  have been neglected in the exponents. This simplification is justified when Gaussian functions are sharply peaked around  $\bar{k}_1$  and  $\bar{k}_2$ , which occurs if the parameter  $\sigma$  is sufficiently small. Due to the fact that  $S_{01,k_1}^u(\bar{k}_1) = 0$  and  $S_{02,k_2}^u(\bar{k}_2) = 0$  define the classical trajectories, the packets are peaked around them. Consequently, both wave packets adhere to the classical trajectories while spreading as  $v_1^2 \rightarrow \infty$  and  $v_2^2 \rightarrow \infty$ . This behavior is evident from the expressions in (70)-(71); the Gaussian widths increase indefinitely due to contributions from terms proportional to  $[S_{01,k_1}^u(\bar{k}_1)]^2$  and  $[S_{02,k_2}^u(\bar{k}_2)]^2$ , as described by the following:

$$S_{01,k_1}^u(\bar{k}_1) = \frac{v_1}{(\bar{k}_1^2 - 1)^{3/2}}, \quad S_{02,k_2}^u(\bar{k}_2) = \frac{iv_2}{(\bar{k}_2^2 - 1)^{3/2}}. \quad (72)$$

The mentioned fact may also be readily recognized from the absolute square of the wave packets

$$|\psi_1(u_1, v_1)|^2 \approx |C_8|^2 \sqrt{\pi} \frac{2\sigma\hbar}{\sqrt{1 + \sigma^4\hbar^2(S_{01,k_1}^u)^2}} \exp \left[ -\frac{\sigma^2 S_{01,k_1}^u{}^2}{1 + \sigma^4\hbar^2(S_{01,k_1}^u)^2} \right], \quad (73)$$

$$|\psi_2(u_2, v_2)|^2 \approx |C_{10}|^2 \sqrt{\pi} \frac{2\sigma\hbar}{\sqrt{1 + \sigma^4\hbar^2(S_{02,k_2}^u)^2}} \exp \left[ -\frac{\sigma^2 S_{02,k_2}^u{}^2}{1 + \sigma^4\hbar^2(S_{02,k_2}^u)^2} \right], \quad (74)$$

where we have neglected the complex conjugate parts in (70)-(71). Consequently, due to the nontrivial dispersion relation—or, more precisely, the non-linear dependence of  $S_{01,k_1}$  and  $S_{02,k_2}$  on  $\bar{k}_1$  and  $\bar{k}_2$ , respectively—spreading effects arise. It follows that the semiclassical approximation is invalid throughout configuration space.

Let us analyze and discuss each sub-state (C- and P-parts) individually.

In approaching to big-rip singularity, we have  $u_2 \rightarrow -\infty$  and  $v_2 \rightarrow -\infty$ . Thus, this singularity dwells in a legitimate quantum region. Due to the fact that

$$v_2^2 \sim \exp \left[ 6\alpha - \sqrt{6}(\lambda_1\varphi_1 + \lambda_2\varphi_2) \right] \equiv e^{6\alpha} V(\varphi_1, \varphi_2),$$

the nontrivial potential causes the dispersion.

As a result, the big-rip singularity is smoothed out—we are no longer able to use an approximate time parameter when wave packets disperse. This marks the end of time and classical evolution, leaving only a stationary quantum state. Such an outcome arises due to the influence of quantum gravity effects at extremely large scales.

Two inequivalent actions will exist for  $u_1 > 0$  (i.e., when  $\lambda_1 < \sqrt{6}$ ). The construction of the wave packets is then based on

$$\begin{aligned} S_{01,k_1} &= k_1 u_1 - \sqrt{k_1^2 - 1} v_1, \\ S_{01,k_1} &= -k_1 u_1 - \sqrt{k_1^2 - 1} v_1. \end{aligned}$$

Furthermore, the entire  $(\alpha, \varphi_1)$ -plane is mapped into a single quarter of the  $(u_1, v_1)$ -plane. However, only one solution meets this requirement—the trivial solution. In order to obtain a nontrivial solution, the boundary condition must be relaxed so that  $\Psi_1 = 0$  is enforced solely at the origin of the  $(u_1, v_1)$ -plane. On the lines  $u_1 = 0$  and  $v_1 = 0$ , the wave packet does not vanish because of the non-normalizability of the wave packet in both  $\alpha$  and  $\varphi_1$ . This stems from the fact that the associated classical trajectory lacks a turning point.

By adopting this adjusted boundary condition, the wave packet vanishes at the big-bang singularity (i.e.,  $\Psi_1 \rightarrow 0$  as  $\alpha \rightarrow -\infty$ ) and spreads out as  $\alpha$  becomes large. This implies that quantum theory avoids the inclusion of a big-bang singularity. It is important to note that since the entire  $(u_2, v_2)$ -plane corresponds to the entire  $(\alpha, \varphi_2)$ -plane, no analogous restriction applies to  $\Psi_2$ . Visual representations of both parts of the wave packet are depicted in Figure 3 in two different ranges.

### 3.4. Quantum quintom cosmology for scalar field fluid and negative cosmological constant

In the model analyzed in subsection 2.4, the classical solutions necessitate a potential structured in the form

$$V(\varphi_1, \varphi_2) = V_{01} \cosh^2 \left( \frac{\varphi_1}{C_{01}} \right) + V_{02} \cosh^2 \left( \frac{\varphi_2}{C_{02}} \right)$$

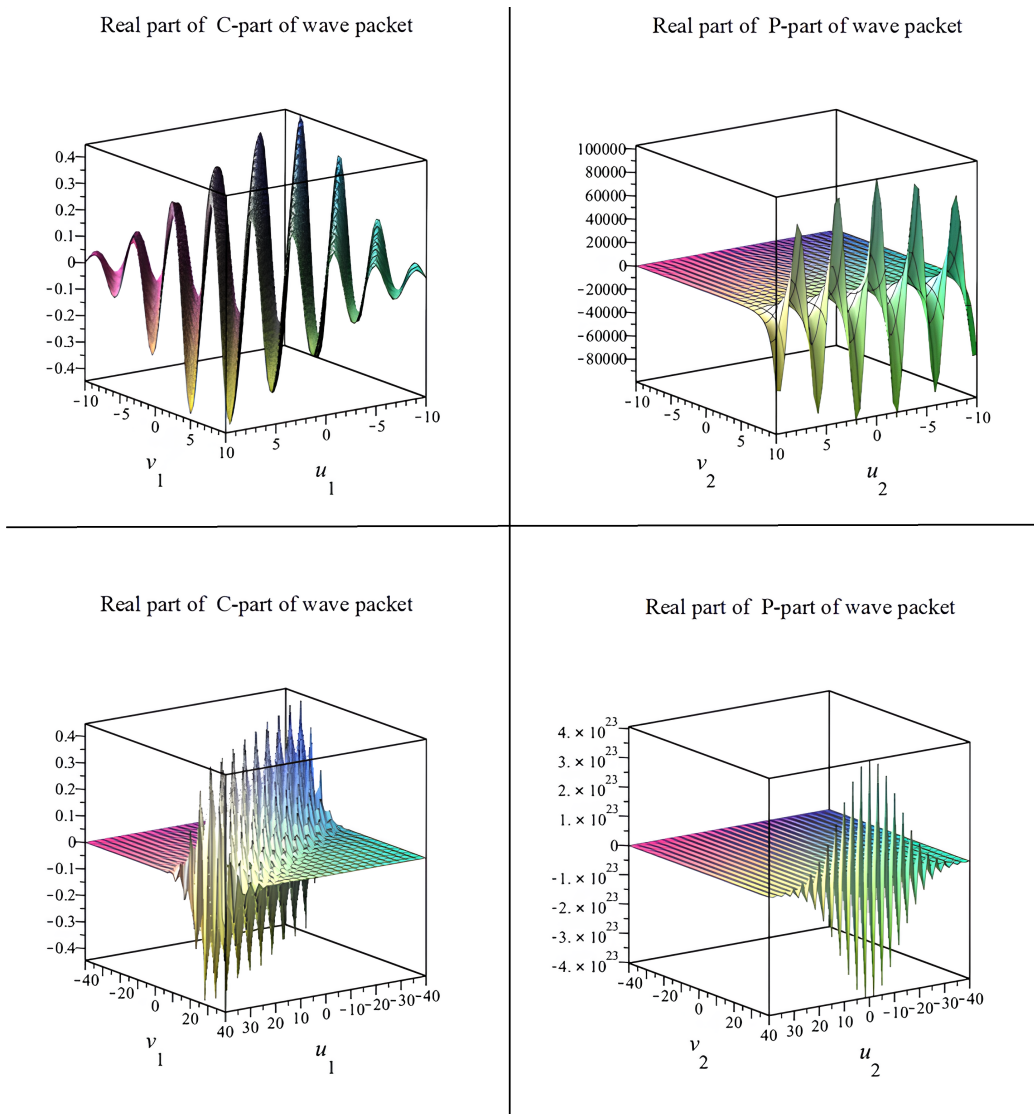


Figure 3: This figure demonstrates the real part of both C- and P-parts of the wave packet in two different ranges for each part. In plotting, we have selected  $\lambda_1 = \sqrt{6}/4$ ,  $\lambda_2 = \sqrt{6}/5$ ,  $\sigma = 0.1$ ,  $\hbar = 1$ ,  $C_8 = \pi^{-1/4}$ , and  $C_{10} = 2\pi^{-1/4}$ .

The Wheeler-DeWitt equation, therefore, takes the form

$$\left[ \frac{\hbar^2}{2} \left( \frac{\partial^2}{\partial \alpha^2} - \frac{\partial^2}{\partial \varphi_1^2} + \frac{\partial^2}{\partial \varphi_2^2} \right) + e^{6\alpha} \left( V_{01} \cosh^2 \left( \frac{\varphi_1}{C_{01}} \right) + V_{02} \cosh^2 \left( \frac{\varphi_2}{C_{02}} \right) + \frac{\Lambda}{6} \right) \right] \Psi(\alpha, \varphi_1, \varphi_2) = 0. \quad (75)$$

Classical singularities are located in a domain where the scalar fields  $|\varphi_1|$  and  $|\varphi_2|$  become large. Therefore, when analyzing quantum behavior in this region, it is adequate to approximate the potential assuming large scalar field values

$$\tilde{V}(\varphi_1, \varphi_2) \approx \frac{V_{01}}{4} e^{\pm 2\varphi_1/|C_{01}|} + \frac{V_{02}}{4} e^{\pm 2\varphi_2/|C_{02}|}, \quad (76)$$

where in the following the upper and lower signs refer to positive and negative scalar fields, respectively. Here, to facilitate the solution process, without loss of generality, we assume  $\Psi(\alpha, \varphi_1, \varphi_2) = \Psi_1(\alpha, \varphi_1)\Psi_2(\alpha, \varphi_2)$ . This approach renders the problem somewhat analogous to the scenario discussed in the previous subsection (see 3.3). Once again, it becomes necessary to apply certain transformations to the variables:

$$\begin{cases} u_1(\alpha, \varphi_1) = 3\sqrt{\frac{V_{01}}{2}} \frac{C_{01}^2 \exp[3\alpha \pm (\varphi_1/|C_{01}|)]}{9C_{01}^2 - 1} \left( \cosh(X_1) \mp \frac{1}{3|C_{01}|} \sinh(X_1) \right); \\ v_1(\alpha, \varphi_1) = 3\sqrt{\frac{V_{01}}{2}} \frac{C_{01}^2 \exp[3\alpha \mp (\varphi_1/|C_{01}|)]}{9C_{01}^2 - 1} \left( \sinh(X_1) \pm \frac{1}{3|C_{01}|} \cosh(X_1) \right); \end{cases} \quad (77)$$

$$\begin{cases} u_2(\alpha, \varphi_2) = 3\sqrt{\frac{V_{02}}{2}} \frac{C_{02}^2 \exp[3\alpha \pm (\varphi_2/|C_{02}|)]}{9C_{02}^2 + 1} \left( \cosh(X_2) \pm \frac{i}{3|C_{02}|} \sinh(X_2) \right); \\ v_2(\alpha, \varphi_2) = 3\sqrt{\frac{V_{02}}{2}} \frac{C_{02}^2 \exp[3\alpha \mp (\varphi_2/|C_{02}|)]}{9C_{02}^2 + 1} \left( -i \sinh(X_2) \pm \frac{1}{3|C_{02}|} \cosh(X_2) \right); \end{cases} \quad (78)$$

where

$$X_1 \equiv 3\varphi_1 \pm \frac{\alpha}{|C_{01}|}, \quad X_2 \equiv i \left( 3\varphi_2 \mp \frac{\alpha}{|C_{02}|} \right). \quad (79)$$

In these variables, the equations (62)-(63) are recovered:

$$\hbar^2 \left( \frac{\partial^2 \Psi_1}{\partial u_1^2} - \frac{\partial^2 \Psi_1}{\partial v_1^2} \right) + \Psi_1 = 0; \quad (80)$$

$$\hbar^2 \left( \frac{\partial^2 \Psi_2}{\partial u_2^2} + \frac{\partial^2 \Psi_2}{\partial v_2^2} \right) + \Psi_2 = 0. \quad (81)$$

Starting from a WKB ansatz, one can derive solutions. The Hamilton-Jacobi equations are, once again, expressed through (64)-(65). It is important to recognize that these equivalences are merely formal, as  $u$  and  $v$  variables were defined differently. These equations can still be effectively solved using (66), with the considerations discussed in subsection 3.3 about the selection of the action being applicable here as well. The equations of motion for

$$\left. \frac{\partial S_{01,k_1}}{\partial k_1} \right|_{k_1=\bar{k}_1} = 0, \quad \left. \frac{\partial S_{02,k_2}}{\partial k_2} \right|_{k_2=\bar{k}_2} = 0,$$

are given by

$$\varphi_{1,\pm}(\alpha) = \mp A \sqrt{\frac{|\beta|}{3|A^2 - 1|}} \alpha + c_{\bar{k}_1}, \quad (82)$$

$$\varphi_{2,\pm}(\alpha) = \pm \sqrt{\frac{|\beta|}{3|A^2 - 1|}} \alpha + c_{\bar{k}_2}, \quad (83)$$

where  $c_{\bar{k}}$ s are constants. These solutions are approximately aligned with the classical solutions (eqs. (34)-(35)). In what follows, we discuss the underlying reasons for this correspondence. First, it is essential to divide our analysis into two parts: CFD and PFD. This distinction arises because, in the former one  $\beta$  is positive, whereas in the latter one it is negative. It is important to note that, due to quantom duality, the behavior of the scalar field differs between the two regimes. For the PFD case, a large scalar field corresponds to a large scalar field, while for CFD one, a large scalar field maps to a small scalar field.

Now, focusing on the PFD regime, if the classical solutions (eqs. (34)-(35)) are approximated for a large scale factor, we find that

$$\varphi_{1,\pm}(\alpha) = \pm A \sqrt{\frac{|\beta|}{3|A^2 - 1|}} \alpha \pm |C_{01}| \ln(2a_2), \quad (84)$$

$$\varphi_{2,\pm}(\alpha) = \pm \sqrt{\frac{|\beta|}{3|A^2 - 1|}} \alpha \pm |C_{02}| \ln(2a_2), \quad (85)$$

where  $\pm$  indicate the distinct branches of the solutions. Given that  $a$  is large, it follows that  $\alpha \geq 0$  in this scenario. Clearly, the limit corresponding to large positive scalar fields lies on the plus-branch, whereas for large negative scalar

fields, it is obtained on the minus-branch.

In the CFD regime, if equations (34)-(35) are approximated for a small scale factor, we arrive at

$$\varphi_{1,\pm}(\alpha) = \pm A \sqrt{\frac{\beta}{3|A^2 - 1|}} \alpha \mp |C_{01}| \ln(2a_2), \quad (86)$$

$$\varphi_{2,\pm}(\alpha) = \pm \sqrt{\frac{\beta}{3|A^2 - 1|}} \alpha \mp |C_{02}| \ln(2a_2). \quad (87)$$

In this scenario,  $\alpha \leq 0$  due to the smallness of  $a$ . As a result, the limit of large positive scalar fields are achieved on the minus-branches, and for large negative scalar fields on the plus-branches.

Therefore, our approximated solutions coincide with classical solutions.

By dint of the classical actions  $S_{01,k_1}$  and  $S_{02,k_2}$ , the C- and P-parts of Wheeler-DeWitt equation can be solved. These equations are precisely satisfied through the WKB ansatz. The resulting wave packets take a similar form to those discussed in the previous subsection; however, this time they involve redefined  $us$  and  $vs$ , along with alternative choices for the centers of the Gaussian functions,  $\bar{k}_1$  and  $\bar{k}_2$ . Just as in the case with vanishing  $\Lambda$ , the sub-wave packets spread as  $v_1^2 \rightarrow \infty$  and  $v_2^2 \rightarrow \infty$ . The big-rip singularity emerges at  $v_2^2 \rightarrow \infty$  and  $u_2 \rightarrow \infty$ . Again, the big-bang singularity does therefore not exist in the quantum theory. Consequently, the singularity remains again hidden in the quantum domain, thereby rendering the semiclassical approximation inapplicable throughout the configuration space. Furthermore, at big-bang,  $\Psi \rightarrow 0$ .

#### 4. Conclusion

Our paper explored the application of standard quantum cosmology formalism, specifically through the Wheeler-DeWitt equation, to scenarios involving quintom field. This investigation is particularly compelling due to the emergence of distinctive features in equation's structure and the presence of scenarios, such as the big-rip singularity at large scale factors in the classical model. Among the most fascinating aspects is the potential manifestation of quantum effects at large scale factors.

The quintom field comprises two components: the ordinary field and the phantom field. As the universe evolves, the dominance between these two

fields can interchange. To address this, the discussion has been divided into two scenarios—one where the canonical field dominates and another where the phantom field is dominant—each scrutinized. For several models, we have analyzed and discussed the classical trajectories within configuration space. Subsequently, we examined the corresponding Wheeler-DeWitt equations, presented various solutions, and explored both the classical limit and the behavior of wave packets that align with the classical trajectories in configuration space.

Utilizing the separation method, the Wheeler-DeWitt equation was split into two coupled equations: one predominantly focusing on the Canonical component (C-part) and the other on the Phantom component (P-part) of the total wave packet. The total wave packet was subsequently represented as the product of these two components.

For the P-part, our findings indicated that these wave packets undergo dispersion near the region of the classical big-rip singularity. As a result, this singularity becomes “smeared out” due to quantum effects at large scale factors. Once the wave packets disperse, it is no longer possible to define an approximate time parameter [53], leading to the termination of classical evolution in a manner free of singularities.

In the C-part, it was observed that the wave packet disappears at the big-bang singularity when suitable boundary conditions were imposed. This effectively eliminates the big-bang singularity from the quantum framework. The result bears similarity to the singularity avoidance seen in loop quantum cosmology [54] and models of shell collapse [55]. Without these boundary conditions, however, the wave packet would merely approach the  $\alpha \rightarrow -\infty$  region without undergoing dispersion. This absence of spreading stems from the Wheeler-DeWitt equation, which behaves like a free wave equation in this particular limit.

## References

- [1] S. Perlmutter et al., *Astrophys. J.* **517** (1999) 565.
- [2] T.R. Choudhury, T. Padmanabhan, *Astron. Astrophys.* **429** (2005) 807.
- [3] D. Huterer and A. Cooray, *Phys. Rev. D* **71** (2005) 023506.
- [4] Supernova Search Team collaboration, *Astrophys. J.* **607** (2004) 665.

- [5] D.A. Dicus, W.W. Repko, Phys. Rev. D **70** (2004) 083527.
- [6] S. W. Hawking, G. F. R. Ellis, The Large Scale Structure of Space-Time (Cambridge University Press, Cambridge, 1973).
- [7] R. R. Caldwell, Phys. Lett. **545** (2002) 23.
- [8] R. R. Caldwell, M. Kamionkowski, N. N. Weinberg, Phys. Rev. Lett. **91** (2003) 071301.
- [9] S. Nojiri, S. D. Odintsov, Phys. Lett. B **562** (2003) 147.
- [10] R. V. Buniy, S. D. H. Hsu, Phys. Lett. B **632** (2006) 543.
- [11] V. A. Rubakov, Theor. Math. Phys. **149** (2006) 1651.
- [12] A. A. Starobinsky, Gravitation Cosmol. **6** (2000) 157.
- [13] V. Gorini, A. Kamenshchik, U. Moschella, V. Pasquier, Phys. Rev. D **69** (2004) 123512.
- [14] J. D. Barrow, Classical Quantum Gravity 21 (2004) L79.
- [15] J. D. Barrow, C. G. Tsagas, Classical Quantum Gravity 22 (2005) 1563.
- [16] S. Nojiri, S. D. Odintsov, Phys. Rev. D **70** (2004) 103522.
- [17] S. Nojiri, S. D. Odintsov, S. Tsujikawa, Phys. Rev. D **71** (2005) 063004.
- [18] C. Armendariz-Picon, V.F. Mukhanov, P.J. Steinhardt, Phys. Rev. Lett. **85** (2000) 4438.
- [19] A. Vikman, Phys. Rev. D **71** (2005) 023515.
- [20] U. Alam, V. Sahni, A.A. Starobinsky, JCAP **06** (2004) 008.
- [21] E. Elizalde, S. Nojiri, S.D. Odintsov, Phys. Rev. D **70** (2004) 043539.
- [22] E.N. Saridakis, J.M. Weller, Phys. Rev. D **81** (2010) 123523.
- [23] Y.-F. Cai, E.N. Saridakis, M.R. Setare, J.-Q. Xia, Phys. Rep. **493** (2010) 1.



- [24] E. Elizalde, S.D. Odintsov, D. Sáez-Gómez, V. Faraoni, Phys. Rev. D **77** (2008) 106005.
- [25] R. Lazkoz, G. Leon, Phys. Lett. B **638** (2006) 303.
- [26] A. Paliathanasis, Universe **8** (2022) 503.
- [27] A. Paliathanasis, G. Leon, Phys. Lett. B **834** (2022) 137407.
- [28] K. Bamba, S. Capozziello, S. Nojiri, S.D. Odintsov, Astrophys. Space Sci. **342** (2012) 155.
- [29] E. Joos et al., Decoherence and the Appearance of a Classical World in Quantum Theory (Springer, Berlin, 2003), 2nd ed.
- [30] C. Kiefer, Quantum Gravity (Clarendon Press, Oxford, 2004).
- [31] M. Bojowald, Ann. Phys. **15** (2006) 326.
- [32] D. Giulini, Phys. Rev. D **51** (1995) 5630.
- [33] D. Giulini, C. Kiefer, Phys. Lett. A **193** (1994) 21.
- [34] C. Kiefer, Phys. Rev. D **38** (1988) 1761.
- [35] S. S. Gousheh, H. R. Sepangi, Phys. Lett. A **272** (2000) 304.
- [36] M. P. Dabrowski, Ann. Phys. **10** (2001) 195.
- [37] C. Kiefer, H. D. Zeh, Phys. Rev. D **51** (1995) 4145.
- [38] M. P. Dabrowski, C. Kiefer, B. Sandhöfer, Phys. Rev. D **74** (2006) 044022.
- [39] J. Khoury, P. J. Steinhardt, and N. Turok, Phys. Rev. Lett. **92** (2004) 031302.
- [40] D. Blais, D. Polarski, Phys. Rev. D **70** (2004) 084008.
- [41] A. A. Coley, R. J. van den Hoogen, Phys. Rev. D **62** (2000) 023517.
- [42] E. J. Copeland, A. Mazumdar, N. J. Nunes, Phys. Rev. D **60** (1999) 083506.

- [43] J. M. Aguirregabiria, A. Chamorro, L. P. Chimento, N. A. Zuccalá, Phys. Rev. D **62** (2000) 084029.
- [44] R. Lazkoz, G. León, Phys. Lett. B **638**, no.4 (2006), 303.
- [45] B. Tajahmad, JCAP **06** (2024) 057.
- [46] S. Basilakos, M. Tsamparlis, A. Paliathanasis, Phys. Rev. D **83** (2011) 103512.
- [47] B. Tajahmad, Ann. Phys. **420** (2020) 168253.
- [48] L. P. Chimento, R. Lazkoz, Int. J. Mod. Phys. D **14** (2005) 587.
- [49] L. P. Chimento, R. Lazkoz, Phys. Rev. Lett. **91** (2003) 211301.
- [50] M. Abramowitz, I. A. Stegun, Handbook of Mathematical Functions (National Bureau of Standards, Washington, 1972), Chap. 9.3.6.
- [51] Ref. [50], Chap. 10.4.59.
- [52] C. Kiefer, Phys. Rev. D **38** (1988) 1761.
- [53] C. Kiefer, Quantum Gravity (Clarendon Press, Oxford, 2004).
- [54] M. Bojowald, Ann. Phys. **15** (2006) 326.
- [55] P. Hájíček, in Quantum Gravity: From Theory to Experimental Search, edited by D. Giulini, C. Kiefer, and C. Lämmerzahl (Springer, Berlin, 2003).